Article

Discovery Medicine 2025; 37(200): 1914–1927
https://doi.org/10.24976/Discov.Med.202537200.165

Osteoprotegerin Promotes Fracture Healing by Enhancing Chondrocyte Differentiation and Activation of the TGF-β Signaling Pathway

Chengbo Wu[1], Xing Lu[2,*]

[1]Department of Trauma II, Yantaishan Hospital, 264001 Yantai, Shandong, China
[2]Department of Trauma I, Yantaishan Hospital, 264001 Yantai, Shandong, China
*Correspondence: ftxz791128@126.com (Xing Lu)
Submitted: 25 April 2025 Revised: 14 August 2025 Accepted: 2 September 2025 Published: 20 September 2025

Background: Fracture healing involves complex cellular and molecular interactions. While osteoprotegerin (OPG) facilitates bone repair by inhibiting osteoclast activity, its role in chondrocyte differentiation and cartilage formation remains unclear. This study examined the effects of OPG on bone and cartilage during fracture repair.

Methods: A murine femoral fracture model was established and treated with subcutaneous injections of OPG recombinant protein or OPG-neutralizing antibodies. Bone healing was assessed by micro-computed tomography (Micro-CT) and Safranin O staining to evaluate callus size and cartilage formation. Immunohistochemistry detected Ace-tubulin, γ-tubulin, Ki-67, and Collagen II expression. qRT-PCR assessed chondrogenic markers, including SRY-box transcription factor 9 (Sox9), Collagen II, Aggrecan, and Collagen X. OPG shRNA was transfected into chondrocytes to evaluate cell viability (CCK-8 assay), Ace-tubulin and γ-tubulin expression (immunofluorescence), and acidic mucopolysaccharides (Alcian blue staining). Western blot was performed to examine the effect of OPG on the Transforming Growth Factor-β (TGF-β) pathway.

Results: OPG expression was significantly elevated during fracture healing ($p < 0.05$). Administration of recombinant OPG increased fracture callus size and improved bone parameters, including bone volume/total volume (BV/TV) ratio, trabecular number (Tb.N), and trabecular thickness (Tb.Th), while reducing trabecular separation (Tb.Sp) ($p < 0.05$). Conversely, OPG blockade produced opposite effects ($p < 0.05$). OPG treatment also upregulated Ace-tubulin, γ-tubulin, Ki-67, Sox9, Collagen II, Aggrecan, and Collagen X ($p < 0.05$), whereas anti-OPG reduced their expression ($p < 0.05$). *In vitro*, OPG knockdown reduced chondrocyte viability, diminished Ace-tubulin and γ-tubulin expression, reduced acidic mucopolysaccharide accumulation, and downregulated chondrogenic markers ($p < 0.05$). Furthermore, OPG silencing suppressed TGF-β signaling by lowering TGF-β1, TGF-βRI, and Smad2/3 phosphorylation ($p < 0.05$).

Conclusions: OPG promotes chondrocyte differentiation and bone formation by regulating TGF-β signaling, highlighting its potential as a therapeutic target for enhancing fracture healing.

Keywords: fracture healing; OPG; chondrocyte differentiation; Collagen II; TGF-β signaling; microtubule dynamics

Introduction

Fractures are common injuries, and their healing process involves a complex interplay of cellular and molecular mechanisms, including bone formation and remodeling [1–3]. During fracture healing, the balance between osteoclast activity and new bone formation is critical. Osteoprotegerin (OPG), a key regulator of bone metabolism, has received considerable attention in recent years [4,5]. OPG is a glycoprotein that functions as a decoy receptor for receptor activator of nuclear factor kappa-B ligand (RANKL), thereby inhibiting osteoclast differentiation and function, and reducing bone resorption [6,7]. However, its role in fracture healing, particularly in chondrocyte differentiation and cartilage formation, remains insufficiently understood.

Previous studies demonstrate that OPG is essential for bone health, and its deficiency, as observed in osteoporosis, is associated with increased bone resorption and fracture risk [8,9]. While the role of OPG in bone metabolism is well established, emerging evidence suggests that it may also influence early endochondral ossification during fracture healing [10,11]. Endochondral ossification involves the formation of cartilage, which is later replaced by bone, and depends on chondrocyte proliferation and differentiation to restore skeletal continuity [12].

The Transforming Growth Factor-β (TGF-β) signaling pathway is another key regulator of fracture healing. TGF-β promotes chondrocyte proliferation and differentiation, facilitating cartilage formation and ultimately bone regeneration [13,14]. Although the interaction between OPG and the TGF-β signaling pathway during fracture healing

has not been extensively characterized, it is hypothesized that OPG may influence this pathway by regulating osteoclast and chondrocyte activity, thereby affecting the efficiency of fracture repair.

This study aims to investigate the role of OPG in fracture healing, with a particular focus on its effects on bone formation and cartilage development. We hypothesize that OPG not only regulates osteoclast activity but also contributes to fracture repair by modulating chondrocyte proliferation, stabilizing microtubule structures, and regulating the TGF-β signaling pathway. By employing recombinant OPG and anti-OPG treatments in a murine fracture model, we aimed to elucidate the molecular mechanisms underlying the role of OPG in bone and cartilage repair. A deeper understanding of the multifaceted roles of OPG in this process may offer novel therapeutic strategies to enhance fracture healing, particularly in cases of delayed or impaired bone regeneration.

Materials and Methods

Animal Experiment

A total of 90 male C57BL/6J mice (6–8 weeks old, 25 $\pm$ 2 g) were obtained from SiPeiFu (Beijing, China). A standardized closed femoral fracture model was established in all mice. General anesthesia was induced by intraperitoneal injection of sodium pentobarbital (57-33-0, Merck, Darmstadt, Germany) at 50 mg/kg body weight. The depth of anesthesia was confirmed by the absence of the pedal withdrawal reflex. Following adequate anesthesia, mice were placed in the supine position on a sterile surgical platform. The right hind limb was shaved and disinfected with 75% ethanol, followed by povidone-iodine. A small incision (~5 mm) was made over the knee, and the distal femur was exposed. A stainless steel pin (0.38 mm diameter) was inserted retrogradely through the intercondylar notch into the femoral canal to provide internal stabilization. A standardized mid-diaphyseal femoral fracture was then induced using a blunt guillotine-like device (fracture forceps). Additional external fixators were applied when necessary. The skin incision was closed with 5-0 absorbable sutures.

After surgery, mice were placed on a heating pad until recovery from anesthesia. Postoperative care included daily monitoring for mobility, wound condition, and signs of pain or distress. Analgesia was provided with buprenorphine (0.05 mg/kg, subcutaneous) every 12 hours for 48 hours. Fracture healing was monitored throughout the study. Mice were randomly assigned into three groups (n = 30 per group): Model group (no treatment; saline) administered subcutaneously, OPG recombinant protein group (100 µg/kg/day, 92526ES60, YEASEN, Shanghai, China) administered subcutaneously, and OPG antibody group (100 µg/kg/day, ab18051, Abcam, Cambridge, UK) administered subcutaneously.

Each experimental group initially included 30 mice. At five designated time points (pre-fracture [days 0], and days 3, 6, 9, and 21 post-fracture), six mice per group were sacrificed for sample collection and analysis. Treatment continued for 21 days in all groups. On days 3, 6, 9, and 21, mice were euthanized by intraperitoneal injection of 3% sodium pentobarbital (110 mg/kg), and callus tissue from the fracture site was harvested for analysis. All animal experiments were approved by the Beijing Maide Kangna Laboratory Animal Welfare Ethics Committee (approval No. MDKN-2024-096).

Micro-CT

Fractured femora were collected, and the surrounding soft tissues were carefully removed. The bone samples were fixed in 10% neutral buffered formalin (60535ES60, YEASEN, Shanghai, China) for at least 24 hours to preserve tissue integrity. Samples were then scanned using a micro-computed tomography (Micro-CT) scanner (Quantum GX2, PerkinElmer, Waltham, MA, USA), with the fracture site centered in the field of view. The scanning range included approximately 3 mm proximal and distal to the fracture, ensuring coverage of the healing tissue and adjacent bone. Micro-CT reconstruction software was used for three-dimensional image reconstruction, generating detailed 3D models of the fracture and healing callus. Subsequently, bone morphometric parameters, including bone volume/total volume (BV/TV) ratio, trabecular number (Tb.N), trabecular thickness (Tb.Th), and trabecular separation (Tb.Sp), were measured and compared among the treatment groups (Model, OPG recombinant protein, and anti-OPG).

Safranin O Staining

Callus tissue sections were prepared and stained using Safranin O (C0621S, Beyotime, Shanghai, China), prepared as a 0.1% aqueous solution. Samples were immersed in the staining solution for approximately 30 minutes to allow for adequate staining, then gently rinsed with distilled water to remove excess dye. Dehydration was performed sequentially using graded ethanol solutions (70%, 85%, 95%, 100%) (64-17-5, Merck, Darmstadt, Germany), soaking for 5 minutes in each concentration. Dehydration was followed by clearing in xylene (1330-20-7, Merck, Darmstadt, Germany), with three immersions of approximately five minutes each. Samples were then mounted with neutral resin to prevent oxidation.

Stained sections were examined under a light microscope (BX53, Olympus, Tokyo, Japan) to evaluate cartilage and bone tissue formation. Quantitative analysis was performed using ImageJ software (version 1.5f, NIH, Bethesda, MD, USA).

Immunohistochemistry (IHC)

Fixed callus tissues were dewaxed, rehydrated, and subjected to heat-induced antigen retrieval. Sections were blocked with 5% BSA blocking solution (ST025, Beyotime, Shanghai, China) to prevent nonspecific binding, followed by overnight incubation at 4 °C with the primary antibodies: Ace-tubulin (ab24610, Abcam, Cambridge, UK), γ-tubulin (ab179503, Abcam, Cambridge, UK), Ki-67 (ab15580, Abcam, Cambridge, UK), and Collagen II (ab307674, Abcam, Cambridge, UK). After washing with PBS, sections were incubated with HRP-labeled secondary antibody (ab6728, Abcam, Cambridge, UK) for 1 hour at room temperature. Color development was achieved using DAB substrate (P0202, Beyotime, Shanghai, China) for 5 minutes at room temperature. Hematoxylin (ST2067, Beyotime, Shanghai, China) was used as a nuclear counterstain, and sections were mounted with mounting medium. Stained sections were visualized under a light microscope (BX53, Olympus, Tokyo, Japan), and quantitative analysis was performed using ImageJ software (version 1.5f, NIH, Bethesda, MD, USA).

Cell Culture

Primary murine chondrocytes (MIC-iCell-s003, Cellverse Co., Ltd., Shanghai, China) were purchased and cultured in DMEM medium (iCell-0001, Cellverse Co., Ltd., Shanghai, China) supplemented with 10% fetal bovine serum (FBS) (C0226, Beyotime, Shanghai, China). Cells were cultured at 37 °C in a humidified atmosphere containing 5% CO_2. Under inverted phase-contrast microscopy, the cultured cells exhibited the characteristic polygonal or rounded morphology of chondrocytes, with distinct cell boundaries and abundant cytoplasm. Cells exhibited strong adherence and proliferative capacity. And mycoplasma testing was negative, confirming culture purity and suitability for downstream experiments.

Cell Transfection

Chondrocytes were seeded at 2–4 $\times$ 10^5 cells per well into a 6-well plate and cultured to 70–80% confluence to ensure optimal conditions for transfection. For gene silencing, either ShRNA negative control (5′-TTCTCCGAACGTGTCACGT TTCAAGAGA ACGTGACACGTTCGGAGAA TTTTT-3′) (Sangon, Shanghai, China) or ShRNA-OPG (5′-GGAUGUACUCAUCUACAAATT TTCAAGAGA UUUGUAGAUGAGUACAUCC TTTTT-3′) (Sangon, Shanghai, China) was diluted in serum-free medium and combined with the transfection reagent Lipofectamine 6000 (C0526FT, Beyotime, Shanghai, China). The mixture was incubated for 20–30 minutes at room temperature to allow formation of transfection complexes.

The complexes were then added to the cell culture medium, and the plates were gently agitated to ensure uniform distribution. Cells were incubated in a 37 °C, 5% CO_2 incubator (ICO Series, Memmert, Stadtilm, Bavaria, Germany) for 8 hours, after which the medium was replaced with fresh complete medium. After 48 hours, transfection efficiency was verified by qPCR analysis of OPG gene expression levels.

Chondrocyte Differentiation

Primary murine chondrocytes were cultured to 80–90% confluence to ensure healthy and optimal growth conditions, typically using cells at the 3rd passage. Cells were seeded at 2–4 $\times$ 10^5 cells per well into a 6-well plate. Differentiation induction medium was prepared as follows: DMEM (iCell-0001, Cellverse Co., Ltd., Shanghai, China), 1 L; 10% FBS (100 mL); TGF-β3 (91705ES, YEASEN, Shanghai, China), 10 ng/mL; Dexamethasone (53269ES, YEASEN, Shanghai, China), 100 nM; Ascorbic acid-2-phosphate (53585ES, YEASEN, Shanghai, China), 50 µg/mL; ITS supplement (Insulin-Transferrin-Selenium) (60708ES, YEASEN, Shanghai, China), 1×; Proline (SM9004, Beyotime, Shanghai, China), 40 µg/mL; Sodium pyruvate (60370ES, YEASEN, Shanghai, China), 1 mM; and Penicillin-streptomycin solution (60162ES, YEASEN, Shanghai, China), 1%. All components were mixed and filter sterilized to ensure uniform distribution.

The existing medium was replaced with the differentiation induction medium, and cultures were maintained at 37 °C in 5% CO_2 for two weeks. Medium was refreshed every three days.

Alcian Blue Staining

Target cells were cultured to 70–80% confluence to ensure healthy growth. Cells were fixed with 4% paraformaldehyde (P0099, Beyotime, Shanghai, China) at room temperature for 20 minutes, then gently washed three times with PBS to remove the fixative. Cells were subsequently stained in 1% Alcian Blue dye (C0153M, Beyotime, Shanghai, China) for 30 minutes. After staining, excess dye was removed by rinsing with PBS. Dehydration was performed sequentially using 70%, 95%, and 100% ethanol, followed by clearing with xylene. Samples were mounted with a neutral mounting medium to avoid bubble formation. Stained cells were observed under a light microscope (BX53, Olympus, Tokyo, Japan). Alcian Blue-positive regions appeared blue, indicating the presence of acidic mucopolysaccharides. Quantitative analysis was performed using ImageJ software (version 1.5f, NIH, Bethesda, MD, USA).

CCK-8 Assay

Transfected cells were cultured in appropriate medium until they reached the logarithmic growth phase, and 5000 cells were seeded into each well of a 96-well plate. The cells were then cultured for 48 hours. Thirty minutes before the end of incubation, 10 µL of CCK-8 reagent (C0037, Beyotime, Shanghai, China) was added to each well and gently

Table 1. Primer sequences used for qRT-PCR.

Primer name	Primer sequence (5′–3′)
mice-OPG-F	TTGGCTGAGTGTTCTGGT
mice-OPG-R	TTGGGAAAGTGGTATGCT
mice-Sox-9-F	ACAACGCAAGCTTCTGCAAG
mice-Sox-9-R	GTGGGGCGAACAAACAAGAC
mice-Col2-F	TCCTACAATGTCAGGGCCAG
mice-Col2-R	TCATCGCAGAGGACATTCCC
mice-Acan-F	AGCCCTTGTCTGAATGGAGC
mice-Acan-R	GTTGGTTTGGACGCCACTTC
mice-Col10-F	CCAGCCGCAAAGAGTCTACAT
mice-Col10-R	AGCACCATCGTTACCACGAG
mice-TGF-βI-F	CCGCAACAACGCAATCTA
mice-TGF-βI-R	TGAGGAGCAGGAAGGGTC
mice-TGF-βRI-F	GAACTCCCAACTACAGGACCTT
mice-TGF-βRI-R	ATGACAGTGCGGTTATGGCA
mice-GAPDH-F	TGTCTCCTGCGACTTCAACA
mice-GAPDH-R	GGTGGTCCAGGGTTTCTTACT

OPG, osteoprotegerin; TGF, Transforming Growth Factor; GAPDH, Glyceraldehyde-3-Phosphate Dehydrogenase.

mixed. The 96-well plate was returned to the incubator and incubated for 2 hours. The absorbance was finally measured at 450 nm using a microplate reader (SpectraMax i3, Molecular Devices, Sunnyvale, CA, USA).

Cell Immunofluorescence

Transfected cells were cultured in DMEM medium until they reached the logarithmic growth phase. The cells were fixed with 4% paraformaldehyde at room temperature for 10 minutes and washed three times with PBS to remove the fixative. They were then treated with 0.1% Triton X-100 at room temperature for 5 minutes to permeabilize the membrane and allow antibodies (Ace-tubulin (66200-1-Ig, Proteintech, Wuhan, China), γ-tubulin (ab11316, Abcam, Cambridge, UK)) to enter the cells, followed by three washes with PBS. Nonspecific binding was blocked by incubation with 5% BSA for 1 hour. The diluted specific primary antibody was added and incubated overnight at 4 °C, followed by three washes with PBS. The Alexa Fluor 594-conjugated secondary antibody (ab150116, Abcam, Cambridge, UK) was then added and incubated at room temperature for 1 hour, followed by three washes to remove unbound antibody. Nuclei were stained with DAPI (C1006, Beyotime, Shanghai, China) for 5 minutes at room temperature and washed three times with PBS. Finally, the cells were mounted with mounting medium and observed under a fluorescence microscope (DMi8, Leica, Wetzlar, Germany).

qRT-PCR

Total RNA was extracted from tissue and cell samples using an RNA extraction kit (R0077S, Beyotime, Shanghai, China). RNA was reverse transcribed into cDNA using a reverse transcription reagent (D7168S, Beyotime, Shanghai, China) and incubated at 37 °C for 1 hour. The qRT-PCR reaction mixture was then prepared, containing the cDNA template, forward and reverse primers, SYBR Green dye, PCR buffer, and DNA polymerase. This mixture was added to a 96-well plate and loaded into a real-time PCR machine (7500 Real-Time PCR System, Applied Biosystems, Foster, CA, USA). The thermal cycling protocol consisted of an initial denaturation at 95 °C for 5 minutes, followed by 40 cycles of 95 °C for 10 seconds and 60 °C for 30 seconds for annealing and extension. A melting curve analysis was then performed. Fluorescence signals were monitored in real-time, and gene expression levels were quantified using the $2^{-\Delta\Delta Ct}$ method relative to a reference gene. Statistical analysis was performed to compare differences between groups. The primer sequences used in this study are listed in Table 1.

Western Blot

Cells and tissues were lysed using RIPA lysis buffer (P0013C, Beyotime, Shanghai, China) supplemented with protease inhibitors to prevent protein degradation. Lysates were incubated on ice for 30 minutes and centrifuged to collect the supernatant. Protein concentration was quantified using the BCA method (P0009, Beyotime, Shanghai, China). During SDS-PAGE (P0012A, Beyotime, Shanghai, China), the appropriate polyacrylamide gel concentration was selected based on protein size. Samples were mixed with SDS loading buffer, heated at 95 °C for 5 minutes to denature the proteins, then loaded and separated by electrophoresis. Proteins were transferred onto a PVDF membrane (FFP24, Beyotime, Shanghai, China), which was blocked with 5% BSA for 1 hour to prevent nonspecific binding. The membrane was incubated overnight at 4 °C with primary antibodies against Smad2/3 (1:1000, ab202445, Abcam, Cambridge, UK), p-Smad2/3 (1:1000, D27F4, Cell Signaling Technology, Denver, MA, USA), and GAPDH (1:1000, ab9485, Abcam, Cambridge, UK). After washing, the membrane was incubated with an HRP-conjugated secondary antibody (1:1000, ab6721, Abcam, Cambridge, UK) at room temperature for 1 hour, followed by additional washing. Protein bands were visualized using an ECL chemiluminescent substrate and detected with a gel imaging system (Gel Doc™, Bio-Rad, Hercules, CA, USA). Band intensities were quantified using ImageJ software (version 1.5f, NIH, Bethesda, MD, USA).

Statistical Analysis

Data analysis was performed using GraphPad Prism (version 9.0, GraphPad Software Inc., San Diego, CA, USA). Statistical comparisons were made using one-way ANOVA. Tukey's post hoc test was applied for multiple comparisons. Results were expressed as mean $\pm$ standard deviation (SD). A p-value < 0.05 was considered statistically significant.

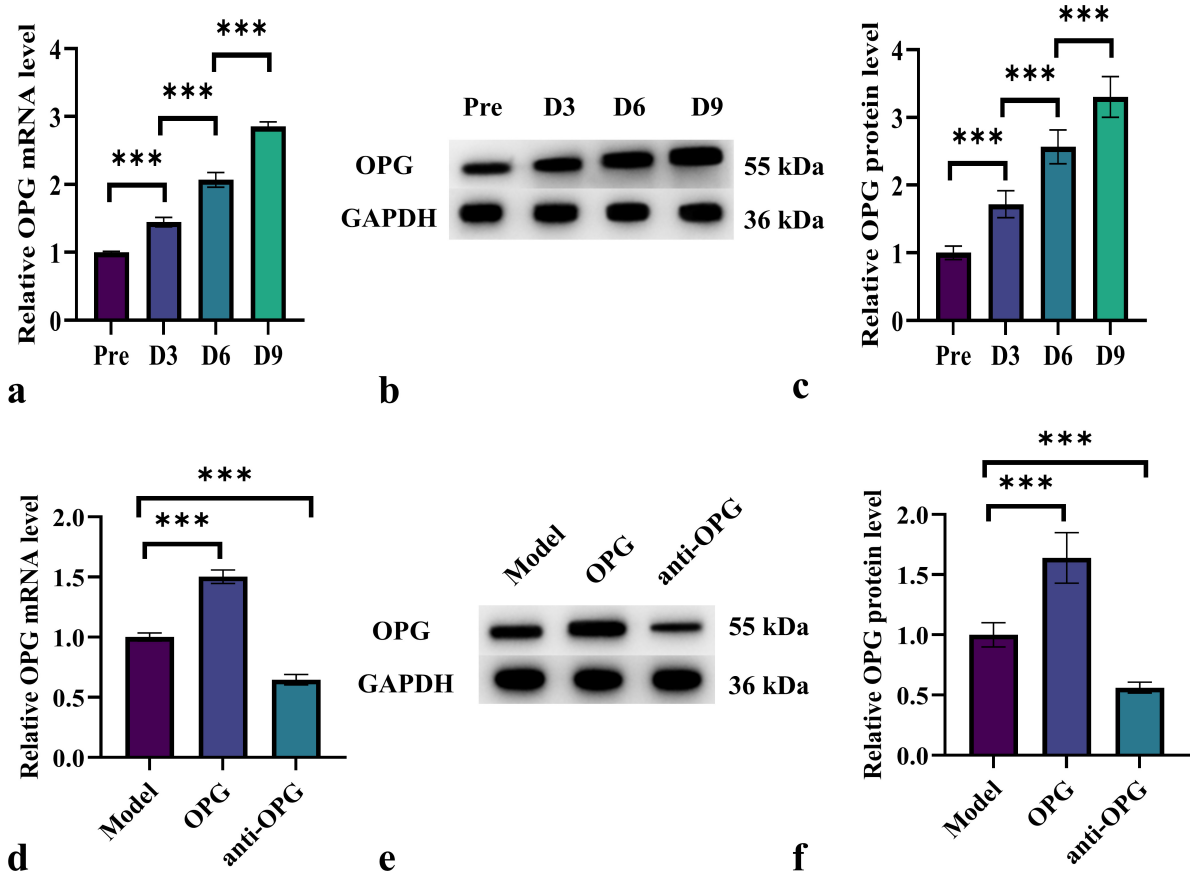

Fig. 1. Increased OPG expression after fracture. (a) Femurs from mice were collected before and after fracture, and qRT-PCR was performed to analyze OPG mRNA expression at the fracture site in the model group. (b,c) Femurs were collected before and after fracture, and Western blot analysis was performed to assess OPG protein expression at the fracture site in the model group. (d) A mouse fracture model was established, and following the fracture, either recombinant OPG protein or anti-OPG was administered. Bone samples were collected on day 9 for qRT-PCR analysis of OPG mRNA expression. (e,f) In the same fracture model, bone samples were collected on day 9 for Western blot analysis of OPG protein expression. n = 6. ***$p < 0.001$.

Results

Increased OPG Expression After Fracture

To determine the expression pattern of OPG, we measured its levels in the callus before and after fracture. As shown in Fig. 1a–c, OPG expression was significantly upregulated at days 3, 6, and 9 post-fracture compared to the pre-fracture baseline ($p < 0.05$). Both mRNA and protein levels of OPG increased gradually over time, reaching peak expression on day 9 post-fracture.

To further evaluate the role of OPG in fracture healing in mice, we administered recombinant OPG protein or anti-OPG antibodies. As shown in Fig. 1d–f, compared to the Model group, the OPG group exhibited significantly higher levels of OPG mRNA and protein, while the anti-OPG group showed a marked decrease in both OPG mRNA and protein levels ($p < 0.05$).

OPG Inhibition Reduces Bone Formation in Fracture Callus

Micro-CT imaging was performed 21 days post-fracture, covering approximately 3 mm proximal and 3 mm distal to the fracture site. The results revealed that, compared to the Model group, the OPG group showed a significant increase in bone volume, while the anti-OPG group exhibited a marked reduction in bone volume, characterized by low bone density and porous woven bone (Fig. 2a). As shown in Fig. 2b–e, the BV/TV ratio, Tb.N, and Tb.Th were significantly higher in the OPG group, while Tb.Sp was significantly lower compared to the Model group ($p < 0.05$). Conversely, the anti-OPG group demonstrated significantly reduced BV/TV ratio, Tb.N, and Tb.Th, accompanied by a significant increase in Tb.Sp ($p < 0.05$).

To assess cartilage formation, Safranin O staining was performed on day 21 post-fracture. As shown in Fig. 3a–d, the OPG group exhibited a significantly larger callus area and greater cartilage volume compared to the Model group, while the anti-OPG group showed a significant reduction

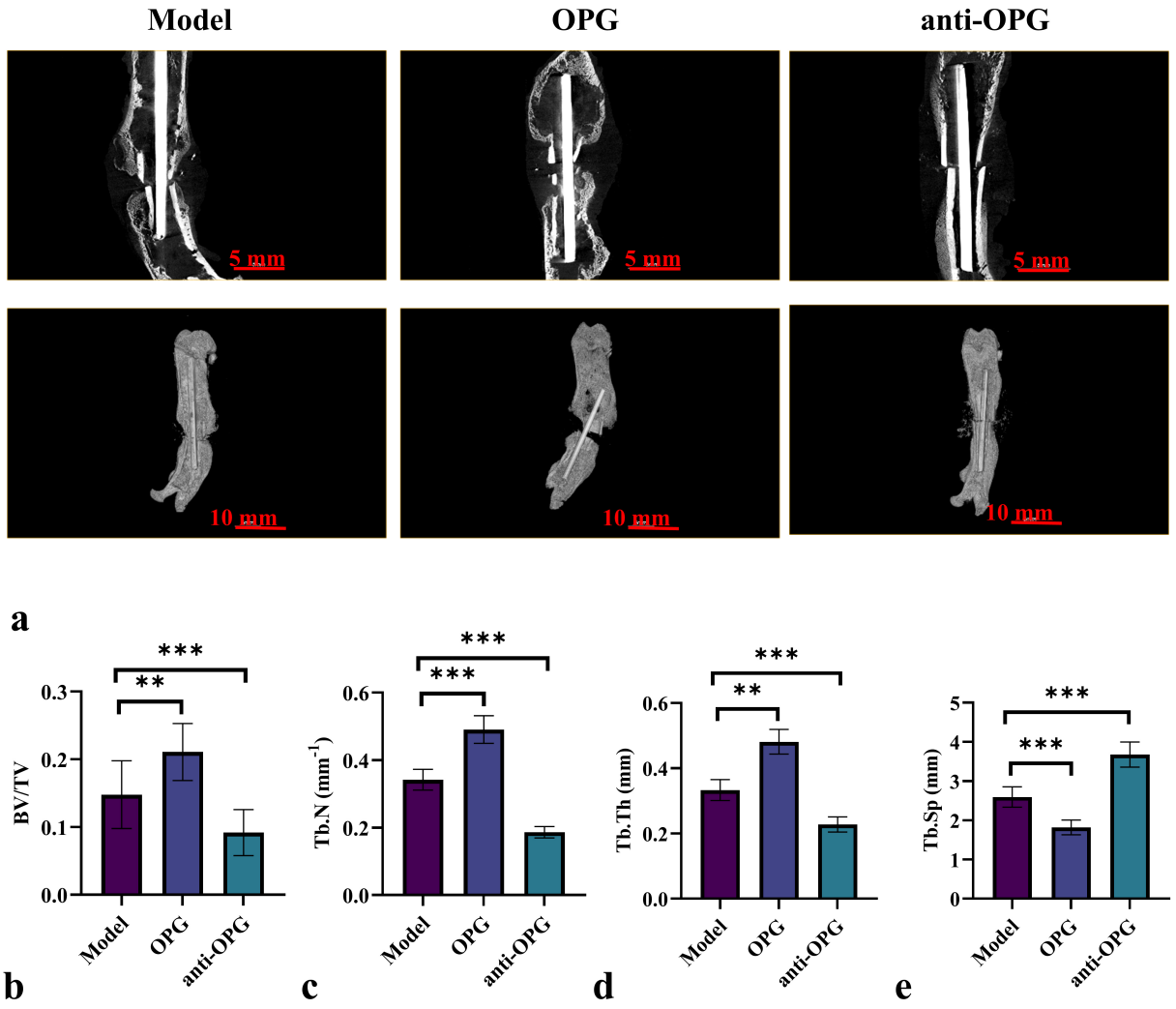

Fig. 2. Micro-computed tomography (Micro-CT) assessment shows that OPG inhibition impairs fracture healing. (a) Representative Micro-CT images of fracture sites obtained 21 days post-fracture. (b) Bone volume/total volume (BV/TV). (c) Trabecular number (Tb.N). (d) Trabecular thickness (Tb.Th). (e) Trabecular separation (Tb.Sp). n = 6. $^{**}p < 0.01$, $^{***}p < 0.001$.

in both callus parameters ($p < 0.05$). Collectively, these findings indicate that OPG inhibition impairs fracture callus and cartilage formation, suggesting that OPG is essential for endochondral ossification during fracture healing.

OPG Inhibition Reduces Microtubule Structure Formation and Chondrogenic Differentiation

To investigate whether OPG inhibition affects microtubule formation during cell division, we examined the expression of Ace-tubulin and γ-tubulin in callus tissue sections using immunohistochemistry on day 9 post-fracture. As shown in Fig. 4a–d, expression of Ace-tubulin and γ-tubulin was significantly elevated in the OPG group compared to the Model group, while the anti-OPG group exhibited a significant reduction in both proteins ($p < 0.05$).

To determine whether OPG inhibition affects chondrocyte proliferation, Ki-67 expression was measured in tissue sections on day 9 post-fracture using immunohistochemistry. The results in (Fig. 4e,f) demonstrated that Ki-67 expression was significantly higher in the OPG group compared to the Model group, while it was markedly reduced in the anti-OPG group ($p < 0.05$).

Additionally, we examined the expression levels of Collagen II on day 9 post-fracture via immunohistochemistry. The findings revealed that Collagen II expression was markedly elevated in the OPG group compared to the Model group, while the anti-OPG group showed significantly reduced expression ($p < 0.05$) (Fig. 4g,h).

Furthermore, the mRNA expression of chondrogenic markers Sox9, Collagen II, Aggrecan, and Collagen X was assessed on day 9 post-fracture. As shown in Fig. 4i–l, recombinant OPG significantly upregulated Sox9, Collagen II, Aggrecan, and Collagen X expression, whereas anti-OPG treatment significantly downregulated their expression ($p < 0.05$).

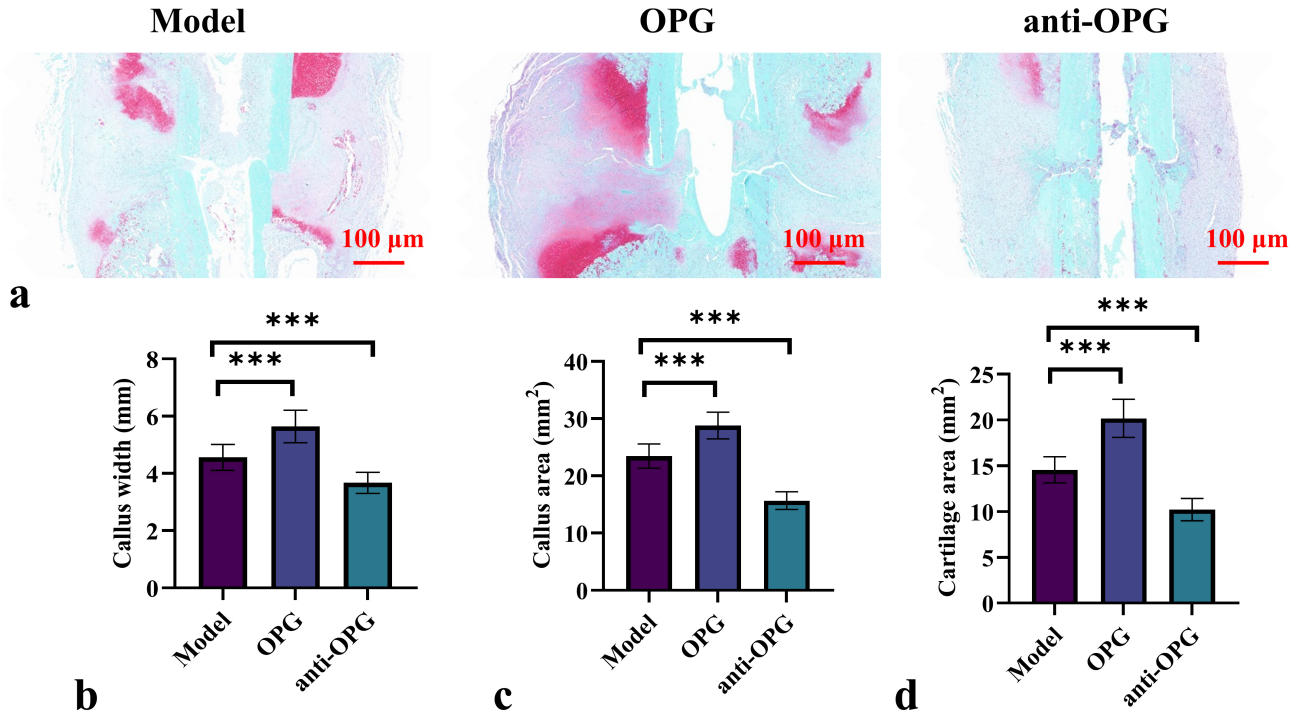

Fig. 3. Histological analysis of fracture callus. (a) Safranin O staining was performed on day 21 post-fracture to evaluate cartilage and proteoglycan content. (b) Callus width. (c) Callus area. (d) Cartilage area. n = 6. ***$p < 0.001$.

OPG Inhibition Reduces Microtubule Structure Formation and Chondrocyte Differentiation In Vitro

In vitro analyses demonstrated that OPG inhibition suppressed microtubule structure formation and impaired chondrocyte differentiation. To further investigate the role of OPG in chondrocyte proliferation and cilium formation, murine chondrocytes were transfected with ShRNA (OPG) to knockdown OPG expression. As shown in Fig. 5a, OPG mRNA expression was significantly reduced in Sh-OPG-transfected chondrocytes ($p < 0.05$). After 48 hours of culture, CCK-8 assay results indicated that OPG knockdown significantly decreased chondrocyte viability ($p < 0.05$) (Fig. 5b). Furthermore, Fig. 5c–f illustrates that, compared to the Sh-NC group, Sh-OPG significantly reduced the expression of Ace-tubulin and γ-tubulin in chondrocytes after 48 hours of growth ($p < 0.05$). To evaluate the role of OPG in chondrogenic differentiation *in vitro*, chondrocytes were infected with Sh-OPG and induced in chondrogenic differentiation medium for 14 days. Sulfated proteoglycan deposition in chondrocytes was detected by Alcian blue staining, which showed a significant decrease in deposition and staining intensity in Sh-OPG-infected chondrocytes ($p < 0.05$) (Fig. 6a,b).

Additionally, OPG knockdown in chondrocytes led to a significant decrease in mRNA levels of Sox9, Collagen II, Aggrecan, and Collagen X ($p < 0.05$) (Fig. 6c–f). Collectively, these findings indicate that OPG inhibition impairs chondrocyte differentiation and downregulates the chondrogenic markers.

OPG Inhibition Impairs Chondrocyte Differentiation by Reducing TGF-β Signaling Activity

We examined the expression of TGF-βI and TGF-βRI mRNA in the fracture callus on day 21 post-fracture. Our findings indicated that recombinant OPG significantly upregulated TGF-βI and TGF-βRI expression in the callus, whereas anti-OPG treatment significantly downregulated their expression ($p < 0.05$) (Fig. 7a,b). Western blot analysis further showed that p-Smad2/3 expression was markedly elevated in the OPG group compared to the Model group, while the anti-OPG group exhibited a significant decrease in p-Smad2/3 levels ($p < 0.05$) (Fig. 7c,d).

In vitro experiments revealed that after 14 days of chondrocyte differentiation, OPG knockdown also significantly reduced the mRNA expression of TGF-βI and TGF-βRI ($p < 0.05$) (Fig. 7e,f). Furthermore, OPG knockdown significantly inhibited the phosphorylation of Smad2/3 ($p < 0.05$) (Fig. 7g,h).

Discussion

This study demonstrates the critical role of OPG in fracture healing, particularly in promoting bone formation and chondrogenesis [15,16]. OPG expression significantly increases following fracture, reaching a peak on day 9, which highlights its vital role during the early and mid-stages of repair. These findings align with previous studies that identified OPG as a key regulatory factor in bone metabolism, acting as a decoy receptor for RANKL to in-

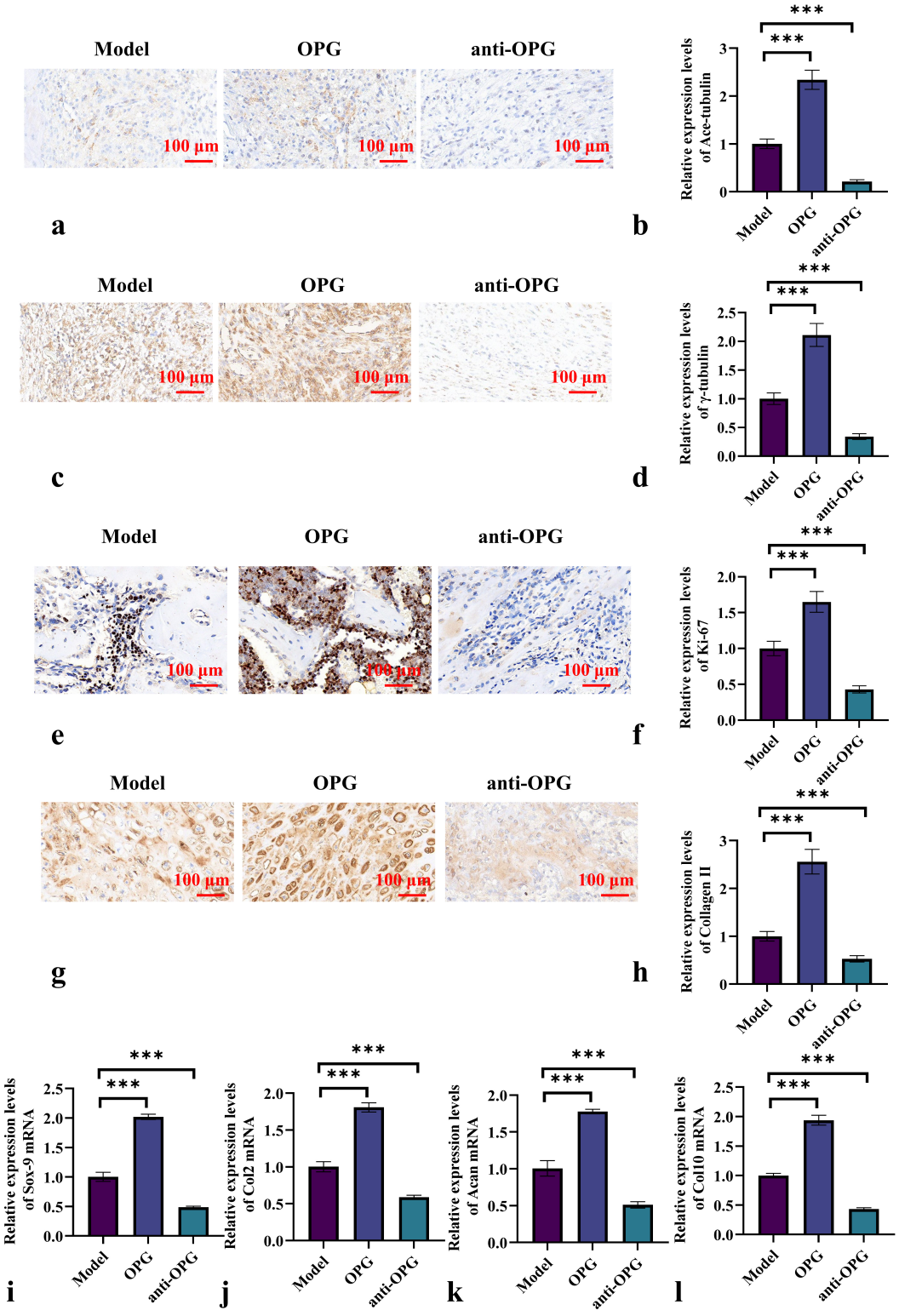

Fig. 4. OPG inhibition reduces microtubule structure formation and chondrogenic differentiation. (a,b) Immunohistochemical analysis of Ace-tubulin expression in fracture callus collected from mice on day 9 post-fracture. (c,d) Immunohistochemical analysis of γ-tubulin expression in fracture callus on day 9 post-fracture. (e,f) Immunohistochemical analysis of Ki-67 expression in fracture callus on day 9 post-fracture. (g,h) Immunohistochemical analysis of Collagen II expression in fracture callus on day 9 post-fracture. (i–l) qPCR analysis of chondrogenic differentiation markers: Sox9 (i), Collagen II (j), Aggrecan (k), and Collagen X (l). n = 6. ***$p < 0.001$.

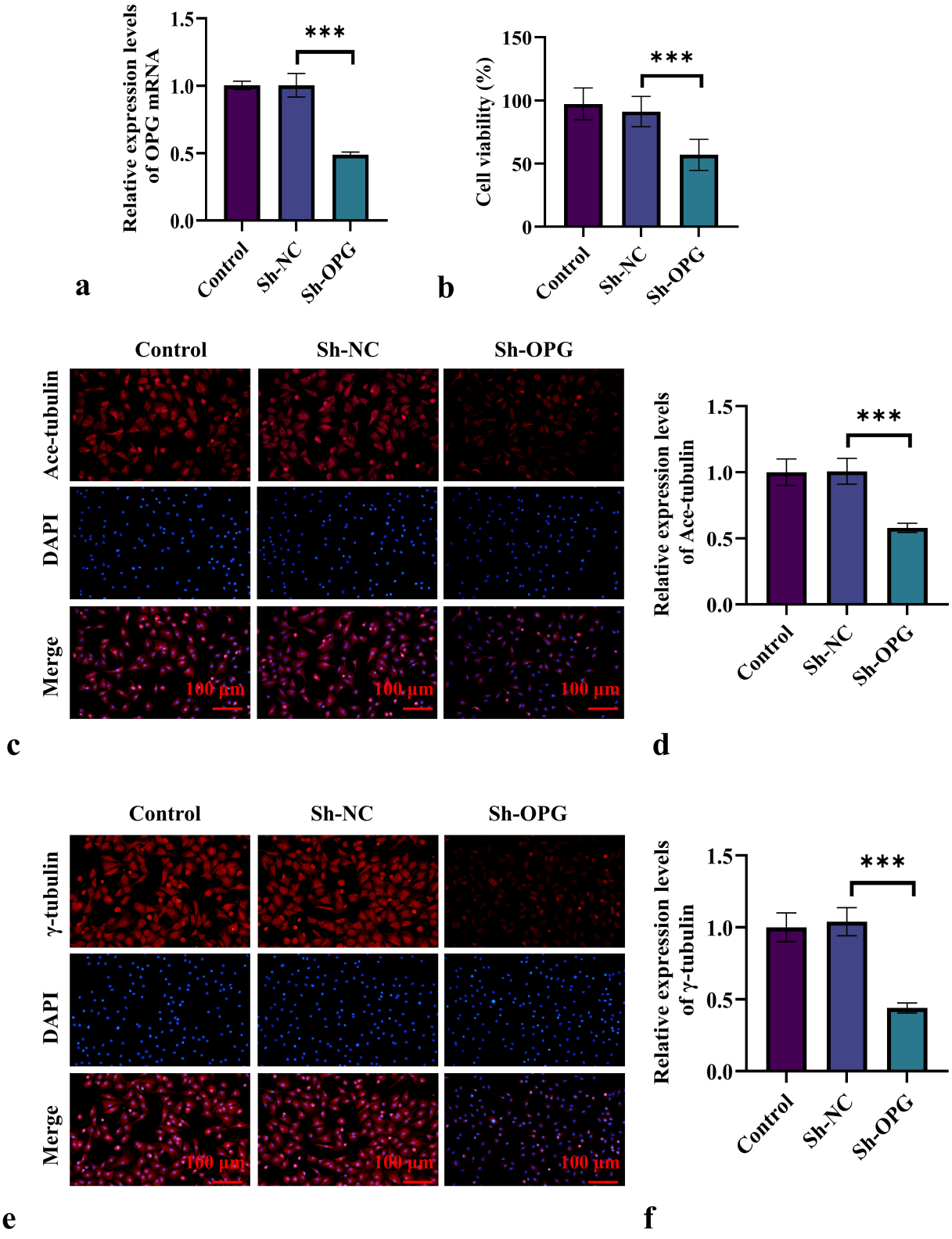

Fig. 5. OPG inhibition reduces microtubule structure formation and chondrocyte differentiation *in vitro*. (a) qRT-PCR analysis of OPG mRNA expression in chondrocytes transfected with Sh-NC or Sh-OPG. (b) CCK-8 assay assessing the effect of OPG knockdown on chondrocyte viability. (c,d) Immunofluorescence analysis of Ace-tubulin expression in chondrocytes following OPG knockdown. (e,f) Immunofluorescence analysis of γ-tubulin expression in chondrocytes following OPG knockdown. n = 6. ***$p < 0.001$.

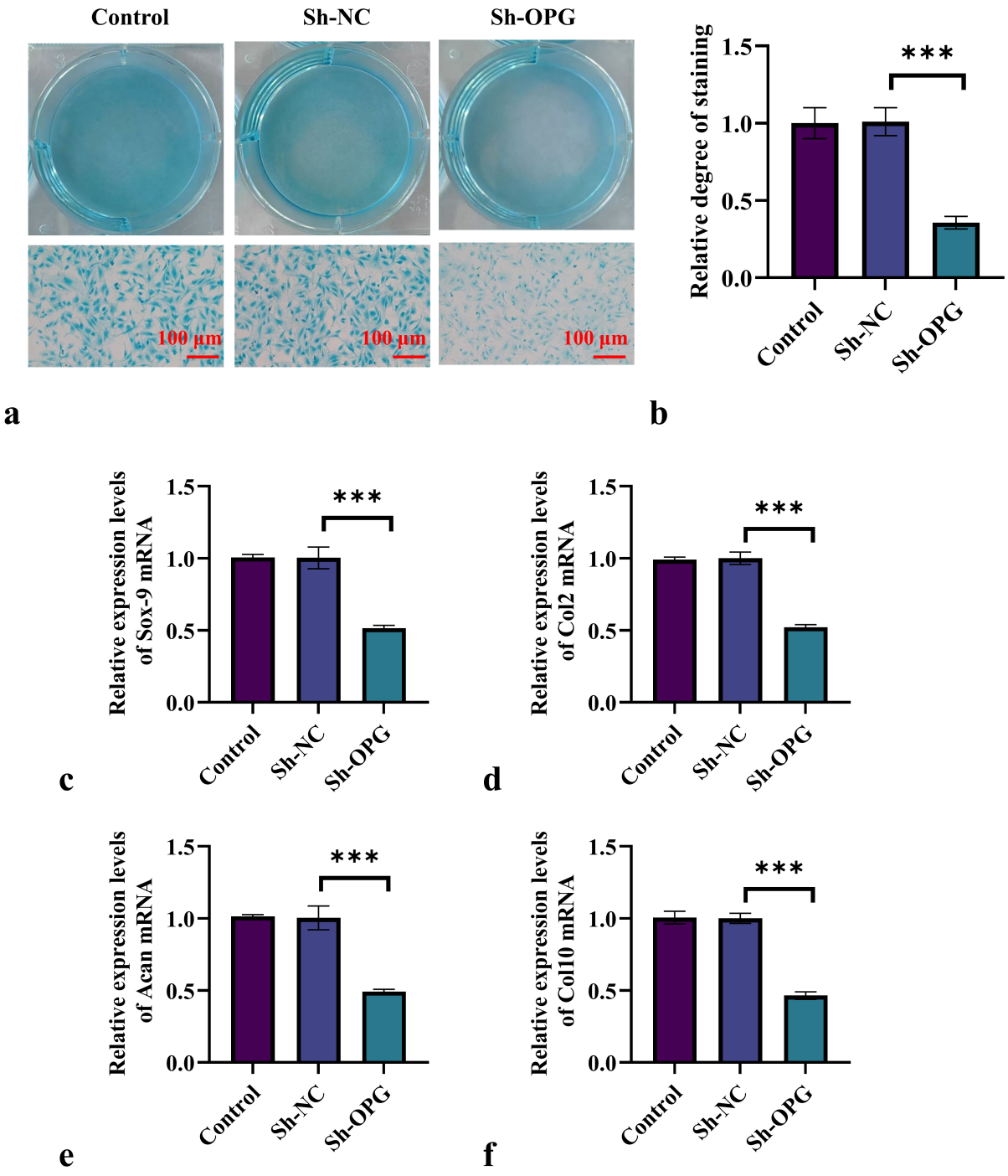

Fig. 6. Inhibition of OPG reduces chondrocyte differentiation *in vitro*. (a,b) Evaluation of proteoglycan production by Alcian Blue staining on day 14 following chondrogenic induction. (c–f) qPCR analysis of chondrogenic differentiation markers: Sox-9, Collagen II, Aggrecan, and Collagen X. n = 6. ***$p < 0.001$.

hibit osteoclastogenesis and thereby prevent excessive bone resorption [4,17]. Our study further expands upon these observations by showing that OPG not only contributes to bone healing but also promotes chondrogenesis during endochondral ossification, an aspect that remains relatively underexplored in the current literature.

The selected dose of 100 μg/kg/day for recombinant OPG protein and anti-OPG antibody was based on previous studies that demonstrated effective modulation of bone metabolism and fracture repair at this concentration without significant adverse effects. This dosage has been widely applied in murine models to achieve sufficient systemic levels of OPG or neutralizing antibodies capable of altering osteo-

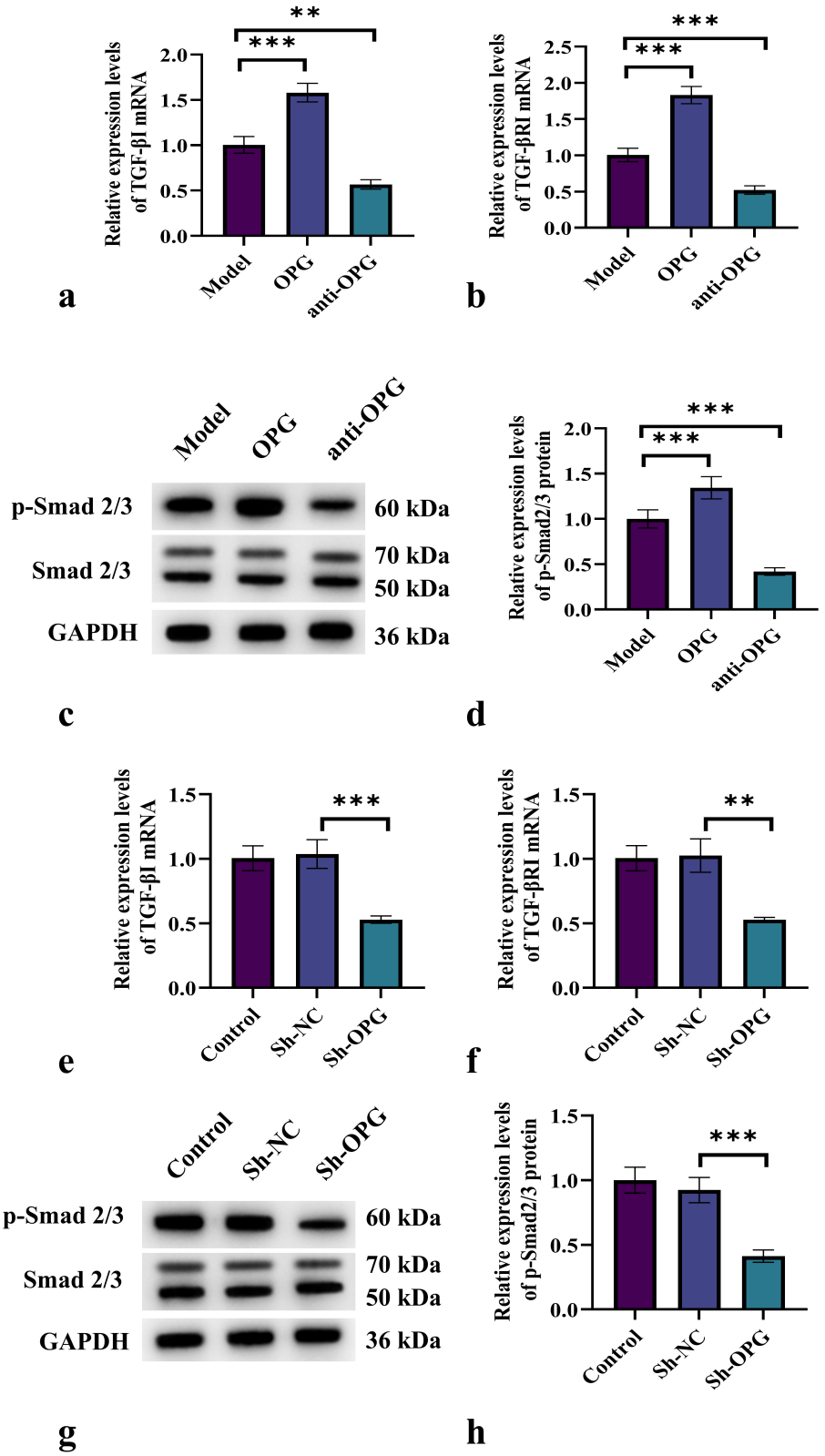

Fig. 7. OPG inhibition impairs chondrocyte differentiation by reducing TGF-β signaling activity. (a) Effect of different treatments on TGF-βI mRNA levels in fracture callus. (b) Effect of different treatments on TGF-βRI mRNA levels in fracture callus. (c,d) Western blot analysis of p-Smad2/3 protein levels in fracture callus. (e) Analysis of TGF-βI mRNA levels in chondrocytes on day 9 post-differentiation after transfection with Sh-NC or Sh-OPG. (f) Analysis of TGF-βRI mRNA levels in chondrocytes on day 9 post-differentiation after transfection with Sh-NC or Sh-OPG. (g,h) Western blot analysis of p-Smad2/3 protein levels during chondrocyte differentiation. n = 6. $^{**}p < 0.01$, $^{***}p < 0.001$.

clast activity and bone remodeling. The treatment duration of 21 days was chosen to coincide with the critical early phase of fracture healing, during which endochondral ossification, callus formation, and remodeling predominantly occur. This period ensures that the administered agents effectively influence the essential biological processes underlying bone regeneration.

Our results confirm that recombinant OPG treatment enhances bone volume, with Micro-CT analysis showing significant improvements in bone volume/total volume (BV/TV) and trabecular microarchitecture. In contrast, anti-OPG administration reduced bone mass and impaired fracture healing, evidenced by decreased trabecular number (Tb.N) and thickness (Tb.Th), together with an increased trabecular separation (Tb.Sp). These findings are consistent with previous studies indicating that OPG deficiency results in heightened osteoclast activity and bone loss [18,19]. Our findings also complement those of Menger *et al*. [20], who reported that OPG application reduces bone resorption and enhances callus formation. Collectively, these results suggest that targeting OPG may represent an effective strategy to improve fracture healing, particularly in cases of osteoporotic fractures or impaired bone regeneration.

The novel finding of this study is the significant role of OPG in chondrogenesis during fracture healing. We observed a marked increase in the expression of chondrogenic markers, including Sox9, Collagen II, Aggrecan, and Collagen X, in the OPG treatment group, indicating that OPG promotes the differentiation and maturation of chondrocytes. Further confirmation was provided by Safranin O staining, which demonstrated increased cartilage callus formation in the OPG group, while anti-OPG treatment resulted in a significant reduction in chondrogenesis. These findings suggest that OPG not only influences late-stage hypertrophic differentiation of chondrocytes but also regulates the proliferation and maturation of early-stage chondrocytes. Its inhibition leads to an overall decrease in differentiation, reflected by the reduction of both early and late markers, rather than merely causing an accumulation of hypertrophic chondrocytes through blockade of hypertrophic differentiation alone. These findings align with previous studies suggesting that OPG contributes to maintaining cartilage homeostasis [21–23]. For instance, Du *et al*. [15] demonstrated that OPG can suppress chondrocyte hypertrophy and matrix degradation. However, our research is the first to directly associate OPG with enhanced chondrogenesis in fracture repair, suggesting a dual role for OPG in supporting both bone and cartilage repair mechanisms.

We also examined the impact of OPG on microtubule dynamics, which are crucial regulators of cell division and differentiation, particularly in chondrocytes. Our immunohistochemical analysis revealed that OPG markedly elevated the expression of Ace-tubulin and γ-tubulin, which are markers of microtubule stability and centrosome organization, respectively. Concurrently, Ki-67 staining revealed increased cellular proliferation. Microtubule stability is essential for normal proliferation and differentiation of chondrocytes, as it provides structural support and coordinates processes required for intramembranous ossification [24,25]. In contrast, OPG inhibition significantly reduced Ace-tubulin and γ-tubulin expression, impairing cell proliferation and microtubule organization, which may contribute to defects in chondrogenesis. These findings suggest that OPG regulates cytoskeletal dynamics essential for chondrocyte function, highlighting the need for further investigation into its role in skeletal tissue repair.

Beyond its regulatory role in microtubule stability and chondrocyte behavior, OPG may also influence key signaling pathways involved in fracture repair. To explore the mechanisms through which OPG contributes to bone and cartilage regeneration, we evaluated its impact on the TGF-β signaling pathway during fracture healing.

OPG treatment markedly elevated the expression of TGF-βI and TGF-βRI, as well as the phosphorylation of Smad2/3, indicating that OPG activates this signaling pathway. Conversely, anti-OPG treatment significantly downregulated TGF-β signaling. The TGF-β pathway plays a pivotal role in promoting chondrocyte proliferation and differentiation during endochondral ossification, and our findings suggest that OPG enhances cartilage and bone formation through activation of this pathway. Previous studies have established that TGF-β signaling is essential for fracture healing, with Smad2/3 phosphorylation serving as a key driver of chondrocyte differentiation and extracellular matrix synthesis [26,27]. Our results align with these observations and provide new insights into the manner in which OPG facilitates tissue repair through the enhancement of TGF-β signaling. Notably, limited research has explored the relationship between OPG and TGF-β signaling in fracture healing, making our findings significant for understanding the broader regulatory mechanisms of OPG in skeletal tissue.

Our findings also align with existing research on the role of OPG in bone metabolism and cartilage health, while expanding upon these previous studies. For instance, the observed increase in bone volume and the improvement of trabecular structure in the OPG treatment group are consistent with the findings of Kram *et al*. [28], who demonstrated that OPG is a potent inhibitor of osteoclastogenesis, thereby reducing bone resorption and enhancing bone density. However, most studies have primarily focused on the anti-resorptive effects of OPG on bone. Our research underscores its additional significance in promoting chondrogenesis and regulating microtubule dynamics, providing a more comprehensive understanding of its role in skeletal tissue repair. Additionally, our observations of reduced TGF-β signaling and impaired chondrocyte proliferation in the OPG inhibition group further confirm the multifaceted regulatory role of OPG during fracture healing, presenting novel insights for future therapeutic strategies.

This study has several limitations. First, the use of a murine fracture model may not fully represent the complexity of human fracture healing, and additional clinical validation is required. Second, the tissue- and cell-specific effects of OPG were not comprehensively examined. Third, only a single dose and fixed treatment duration were applied, without assessing dose dependence or the optimal therapeutic window. Fourth, although OPG was shown to influence the TGF-β signaling pathway, mechanistic validation was limited. Finally, potential systemic side effects and long-term safety of OPG treatment were not evaluated. Future studies should aim to validate these findings in larger animal models and eventually in clinical settings to better evaluate the translational potential of OPG-based therapies. Further investigation is also required to delineate the tissue- and cell-specific roles of OPG during fracture healing, particularly its interactions with osteoblasts, osteoclasts, and chondrocytes. Exploring a broader range of OPG doses and treatment durations will help determine the optimal therapeutic window. In addition, mechanistic studies utilizing pathway inhibitors or genetic models are warranted to clarify the precise molecular mechanisms through which OPG regulates chondrocyte differentiation and the TGF-β signaling pathway. Finally, the long-term safety and systemic consequences of OPG administration should be comprehensively evaluated to ensure clinical applicability.

The findings of this study suggest that OPG represents a promising therapeutic target for enhancing fracture healing, particularly in conditions where bone and cartilage repair are impaired, such as in osteoporosis or delayed fracture healing. The dual role of OPG in promoting bone formation and chondrogenesis, along with its regulation of key signaling pathways such as TGF-β, positions it as a potential candidate for therapeutic intervention, especially in combination therapies. Future research should investigate the long-term effects of OPG modulation in clinical fracture healing models and further explore its interactions with other essential regulators of bone and cartilage repair.

Conclusions

In summary, this study provides new insights into the multifaceted role of OPG in fracture healing. OPG promotes bone formation not only by suppressing osteoclastogenesis but also by enhancing chondrocyte proliferation, microtubule stability, and TGF-β signaling, thus supporting the repair of both cartilage and bone. Inhibition of OPG leads to impaired healing of bone and cartilage, highlighting its essential role in skeletal repair. These findings lay a foundation for therapeutic strategies aimed at improving fracture healing by targeting OPG and its associated pathways.

Availability of Data and Materials

The data that support the findings of this study are available from the corresponding author upon reasonable request.

Author Contributions

CBW and XL designed the research study. CBW performed the research. CBW and XL provided advice on the experiments. XL analyzed the data. CBW and XL drafted the manuscript. Both authors contributed to important editorial changes in the manuscript. Both authors read and approved the final manuscript. Both authors have participated sufficiently in the work and agreed to be accountable for all aspects of the work.

Ethics Approval and Consent to Participate

The study has been approved by the Beijing Maide Kangna Laboratory Animal Welfare Ethics Committee (approval No. MDKN-2024-096).

Acknowledgment

Not applicable.

Funding

This research received no external funding.

Conflict of Interest

The authors declare no conflict of interest.

References

[1] Mick P, Fischer C. Delayed Fracture Healing. Seminars in Musculoskeletal Radiology. 2022; 26: 329–337. https://doi.org/10.1055/s-0041-1740380.

[2] Baertl S, Alt V, Rupp M. Surgical enhancement of fracture healing - operative vs. nonoperative treatment. Injury. 2021; 52: S12–S17. https://doi.org/10.1016/j.injury.2020.11.049.

[3] Breulmann FL, Hatt LP, Schmitz B, Wehrle E, Richards RG, Della Bella E, *et al*. Prognostic and therapeutic potential of microRNAs for fracture healing processes and non-union fractures: A systematic review. Clinical and Translational Medicine. 2023; 13: e1161. https://doi.org/10.1002/ctm2.1161.

[4] Udagawa N, Koide M, Nakamura M, Nakamichi Y, Yamashita T, Uehara S, *et al*. Osteoclast differentiation by RANKL and OPG signaling pathways. Journal of Bone and Mineral Metabolism. 2021; 39: 19–26. https://doi.org/10.1007/s00774-020-01162-6.

[5] Nishida D, Arai A, Zhao L, Yang M, Nakamichi Y, Horibe K, *et al*. RANKL/OPG ratio regulates odontoclastogenesis in damaged dental pulp. Scientific Reports. 2021; 11: 4575. https://doi.org/10.1038/s41598-021-84354-y.

[6] Hooshiar SH, Tobeiha M, Jafarnejad S. Soy Isoflavones and Bone Health: Focus on the RANKL/RANK/OPG Pathway. BioMed Research International. 2022; 2022: 8862278. https://doi.org/10.1155/2022/8862278.

[7] Wan Y, Hu C, Hou Y, Si C, Zhao Q, Wang Z, *et al*. OPG gene-modified adipose-derived stem cells improve bone formation around implants in osteoporotic rat maxillae. Heliyon. 2023; 9: e19474. https://doi.org/10.1016/j.heliyon.2023.e19474.

[8] Han X, Zheng L, Mu YY, Li HZ, He XF. Association between *OPG* polymorphisms and osteoporosis risk: An updated meta-analysis. Frontiers in Genetics. 2022; 13: 1032110. https://doi.org/10.3389/fgene.2022.1032110.

[9] Yasuda H. Discovery of the RANKL/RANK/OPG system. Journal of Bone and Mineral Metabolism. 2021; 39: 2–11. https://doi.org/10.1007/s00774-020-01175-1.

[10] Ren Q, Zhang W, Li P, Zhou J, Li Z, Zhou Y, *et al*. Up-regulation of osteoprotegerin inhibits *tert*-butyl hydroperoxide-induced apoptosis of human chondrocytes. Experimental and Therapeutic Medicine. 2022; 24: 470. https://doi.org/10.3892/etm.2022.11397.

[11] Qin Y, Shirakawa J, Xu C, Chen R, Yang X, Ng C, *et al*. Long non-coding RNA *Malat1* fine-tunes bone homeostasis and repair by orchestrating cellular crosstalk and β-catenin-OPG/Jagged1 pathway. eLife. 2024; 13: RP98900. https://doi.org/10.7554/eLife.98900.

[12] Bačenková D, Trebuňová M, Demeterová J, Živčák J. Human Chondrocytes, Metabolism of Articular Cartilage, and Strategies for Application to Tissue Engineering. International Journal of Molecular Sciences. 2023; 24: 17096. https://doi.org/10.3390/ijms242317096.

[13] Ying J, Ge Q, Hu S, Luo C, Lu F, Yu Y, *et al*. Amygdalin Promotes Fracture Healing through TGF-β/Smad Signaling in Mesenchymal Stem Cells. Stem Cells International. 2020; 2020: 8811963. https://doi.org/10.1155/2020/8811963.

[14] Yao L, Lu J, Zhong L, Wei Y, Gui T, Wang L, *et al*. Activin A marks a novel progenitor cell population during fracture healing and reveals a therapeutic strategy. eLife. 2023; 12: e89822. https://doi.org/10.7554/eLife.89822.

[15] Du G, Xiang C, Sang X, Wang X, Shi Y, Wang N, *et al*. Histone deacetylase 4 deletion results in abnormal chondrocyte hypertrophy and premature ossification from collagen type 2α1 expressing cells. Molecular Medicine Reports. 2020; 22: 4031–4040. https://doi.org/10.3892/mmr.2020.11465.

[16] Chen X, Wang Y, Chen R, Qu N, Zhang B, Xia C. Suppressing PLCγ1 enhances osteogenic and chondrogenic potential of BMSCs. Biochemical and Biophysical Research Communications. 2020; 532: 292–299. https://doi.org/10.1016/j.bbrc.2020.08.049.

[17] Tobeiha M, Moghadasian MH, Amin N, Jafarnejad S. RANKL/RANK/OPG Pathway: A Mechanism Involved in Exercise-Induced Bone Remodeling. BioMed Research International. 2020; 2020: 6910312. https://doi.org/10.1155/2020/6910312.

[18] Kim JM, Lin C, Stavre Z, Greenblatt MB, Shim JH. Osteoblast-Osteoclast Communication and Bone Homeostasis. Cells. 2020; 9: 2073. https://doi.org/10.3390/cells9092073.

[19] Ono T, Hayashi M, Sasaki F, Nakashima T. RANKL biology: bone metabolism, the immune system, and beyond. Inflammation and Regeneration. 2020; 40: 2. https://doi.org/10.1186/s41232-019-0111-3.

[20] Menger MM, Stief M, Scheuer C, Rollmann MF, Herath SC, Braun BJ, *et al*. Diclofenac, a NSAID, delays fracture healing in aged mice. Experimental Gerontology. 2023; 178: 112201. https://doi.org/10.1016/j.exger.2023.112201.

[21] Luo Y, Li M, Xu D. Biochemical characterization of a disease-causing human osteoprotegerin variant. Scientific Reports. 2022; 12: 15279. https://doi.org/10.1038/s41598-022-19522-9.

[22] Chen W, Wang Q, Tao H, Lu L, Zhou J, Wang Q, *et al*. Subchondral osteoclasts and osteoarthritis: new insights and potential therapeutic avenues. Acta Biochimica et Biophysica Sinica. 2024; 56: 499–512. https://doi.org/10.3724/abbs.2024017.

[23] Yan J, Feng G, Yang Y, Ding D, Ma L, Zhao X, *et al*. Autophagy attenuates osteoarthritis in mice by inhibiting chondrocyte pyroptosis and improving subchondral bone remodeling. Biomolecules & Biomedicine. 2023; 23: 77–88. https://doi.org/10.17305/bjbms.2022.7677.

[24] Li J, Fan C, Lv Z, Sun Z, Han J, Wang M, *et al*. Microtubule stabilization targeting regenerative chondrocyte cluster for cartilage regeneration. Theranostics. 2023; 13: 3480–3496. https://doi.org/10.7150/thno.85077.

[25] Quadri N, Upadhyai P. Primary cilia in skeletal development and disease. Experimental Cell Research. 2023; 431: 113751. https://doi.org/10.1016/j.yexcr.2023.113751.

[26] Kim D, Kim JE, Lee SB, Lee NY, Park SY. Gulp1 regulates chondrocyte growth arrest and differentiation via the TGF-β/SMAD2/3 pathway. FEBS Letters. 2024; 598: 935–944. https://doi.org/10.1002/1873-3468.14862.

[27] Wu M, Wu S, Chen W, Li YP. The roles and regulatory mechanisms of TGF-β and BMP signaling in bone and cartilage development, homeostasis and disease. Cell Research. 2024; 34: 101–123. https://doi.org/10.1038/s41422-023-00918-9.

[28] Kram V, Jani P, Kilts TM, Li L, Chu EY, Young MF. OPG-Fc treatment partially rescues low bone mass phenotype in mature Bgn/Fmod deficient mice but is deleterious to the young mouse skeleton. Journal of Structural Biology. 2020; 212: 107627. https://doi.org/10.1016/j.jsb.2020.107627.